31st International Conference Nuclear Energy for New Europe
NENE 2022 September 12-15 PORTOROŽ SLOVENIA

Implementation and Validation of the Steady State SP_3 Approximation in the GRS Code FENNECS

Silvia lo Muzio
Gesellschaft für Anlagen- und Reaktorsicherheit (GRS) gGmbH
Boltzmannstr. 14
85748 Garching near Munich, Germany
silvia.lomuzio@grs.de

Armin Seubert
Gesellschaft für Anlagen- und Reaktorsicherheit (GRS) gGmbH
Boltzmannstr. 14
85748 Garching near Munich, Germany
armin.seubert@grs.de

ABSTRACT

From the worldwide growing interest in Small Modular Reactors (SMRs) and Micro Modular Reactors (MMRs), it arises the necessity to employ a proper neutronic calculation tool for their safety assessment. Most of the deterministic neutronic solvers rely on the diffusion approximation that is derived assuming isotropic scattering, low probability of neutron absorption compared to scattering, as well as a weakly varying neutron flux in space. This last assumption may not hold for small cores, like the ones of SMRs and MMRs: here, due to their reduced size and often their heterogeneity, high neutron flux gradients are present. An alternative to the use of the diffusion equation is the application of the third order Simplified Spherical Harmonics (SP_3) approximation of the neutron transport equation, which is expected to perform better for SMRs and MMRs.

For this reason, the Finite ElemeNt NeutroniCS (FENNECS) code, currently under development at GRS, which already provides a diffusion solver, was expanded by a steady state SP_3 solver. FENNECS offers a high geometrical flexibility, which is essential to model complex systems like SMRs and MMRs.

In this paper, starting from the transport equation, the steady state SP_3 approximation of the neutron transport equation is derived. Then, in order to implement the SP_3 equations in the FENNECS code, which is based on the Finite Element Method, these are cast into the Galerkin (weak) form. Finally, based on benchmark exercises, the correct functionality of the SP_3 solver implemented in FENNECS is shown.

1 INTRODUCTION

The neutron transport equation describes the neutron population in a medium. Here, taking into account the spatial as well as the angular dependency, the neutrons sinks and sources are described. On one hand, thanks to its exact description of the phenomena, very accurate results can be obtained. On the other hand, to solve the transport equation using deterministic or with Monte Carlo codes is computationally expensive in both cases. This problem can be solved, by applying approximations [1–4].

The most commonly used approximation of the transport equation is diffusion theory. This is based on three assumptions, which are isotropic scattering, a very small probability of absorption compared to scattering ($\Sigma_a \ll \Sigma_s$), and a weak variation of the neutron flux in space (in particular, the neutron current is proportional to the flux gradient according to Fick's law). The first criterion is fulfilled only by heavy nuclei. The second one is not true for fuel and control materials. Finally, the last assumption is satisfied for homogeneous and large media (with respect to the mean free path length $\bar{\lambda}_n$) at a distance of a few $\bar{\lambda}_n$ away from the boundary. Consequently, this approximation may not be applicable near material interfaces and for small cores, like (v)SMR and MMR [5–7].

For the safety assessment of these systems, an appropriate approximation to the neutron transport equation is essential. One suited candidate is the Simplified Spherical Harmonics approximation of third order, or SP_3. This can be derived expanding the angular terms of the transport equation with Legendre's polynomials, even in 3D, without performing the transition to spherical harmonics [4,8,9].

In order to model (v)SMR and MMR, the Finite ElemeNt NeutroniCS (FENNECS) code, outlined in section 2, must be extended by an SP_3 solver. For this reason, in section 3, the steady state SP_3 approximation in the Galerkin (weak) form, as it is already used for the FENNECS diffusion solver, is derived. Finally, in section 4, validation with benchmark exercises is performed.

2 FENNECS

FENNECS was recently developed at Gesellschaft für Anlagen- und Reaktorsicherheit gGmbH (GRS). Originally, it was a 3D few group finite element based diffusion code, capable to model steady state as well as transient core configurations. FENNECS is based on the Galerkin weighted residual approach, where upright triangular prisms with linear basis functions are used as spatial elements. Due to its geometrical flexibility, it is capable to model complex and irregular geometries, like most often occurring in various (v)SMR and MMR concepts. The spatial meshing is performed by the Python Enhanced Meshing Tool with YAML input, PEMTY. To run the calculations, cross section libraries in NEMTAB format are applied [10,11].

3 DERIVATION OF THE STEADY STATE SP_3 APPROXIMATION IN THE GALERKIN FORMALISM

The SP_3 approximation is derived from the one dimensional transport equation, which can be found in [6] and [12], having G discretized energy groups, as in [13], where $g\epsilon(1,\dots,G)$ and $g = 1$ is the lowest energy group. Firstly, to obtain the Spherical Harmonics approximation of third order (P_3), the variables showing an angular dependency are expanded with Legendre polynomials up to the third order, as in [12]. Similarly to [13], also here it is assumed that higher order scattering between energy groups is neglected. Hence, between different energy groups only the zeroth order scattering is considered. By doing a first step towards the spatial finite elements discretization, it is assumed that all nuclear data are constant within a finite element e. From the one-dimensional P_3 equations, the three-dimensional SP_3 approximation can be obtained by keeping the Legendre expansions, by simply replacing the double derivative with the Laplacian and the x -dependency with $\vec{r}$. For the even order neutron fluxes, hence ϕ_0, which is the scalar flux, and ϕ_2, the following notations are used:

$$F_{0,g}(\vec{r}) = \phi_{0,g}(\vec{r}) + 2\phi_{2,g}(\vec{r}) \tag{1}$$

$$F_{1,g}(\vec{r}) = \phi_{2,g}(\vec{r}). \tag{2}$$

Finally, the following formulation of the SP_3 system of equations is obtained:

$$-\Delta F_{0,g}(\vec{r})D^e_{0,g} + F_{0,g}(\vec{r})\left(\Sigma^e_{t,g} - \Sigma^e_{s,0,gg}\right) - 2F_{1,g}(\vec{r})\left(\Sigma^e_{t,g} - \Sigma^e_{s,0,gg}\right) = S_{0,g}(\vec{r}), \quad \forall\, \vec{r} \in e \tag{3}$$

$$-\frac{2}{3}F_{0,g}(\vec{r})\left(\Sigma^e_{t,g} - \Sigma^e_{s,0,gg}\right) - \Delta F_{1,g}(\vec{r})D^e_{1,g} + F_{1,g}(\vec{r})\left(\frac{4}{3}\left(\Sigma^e_{t,g} - \Sigma^e_{s,0,gg}\right) + \frac{5}{3}\left(\Sigma^e_{t,g} - \Sigma^e_{s,2,gg}\right)\right) = -\frac{2}{3}S_{0,g}(\vec{r}), \forall\, \vec{r} \in e \tag{4}$$

where

$$S_{0,g}(\vec{r}) = \frac{\chi_g}{k_{eff}}\sum_{g'=1}^{G}\vartheta\Sigma^e_{f,g'}\left(F_{0,g'}(\vec{r}) - 2F_{1,g'}(\vec{r})\right) + \sum_{g'=1,g'\neq g}^{G}\Sigma^e_{s,0,g'g}\left(F_{0,g'}(\vec{r}) - 2F_{1,g'}(\vec{r})\right), \forall\, \vec{r} \in e. \tag{5}$$

Here, the variables with the apostrophe describe the neutron state after the scattering event. ϑ is the fission yield and Σ_t, Σ_s and Σ_f are the total, scattering and fission macroscopic cross sections, respectively. In Eq. (5), χ_g and k_{eff} are the group fission spectrum and the effective multiplication factor, respectively. Furthermore, in Eq. (3) and (4), $D_{0,g}$ and $D_{1,g}$ are the zeroth and first order diffusion coefficients, defined as

$$D_{0,g} = \frac{1}{3\left(\Sigma_{t,g} - \Sigma_{s,1,gg}\right)} \tag{6}$$

$$D_{1,g} = \frac{3}{7\left(\Sigma_{t,g} - \Sigma_{s,3,gg}\right)}. \tag{7}$$

The Galerkin (weak) form can be obtained following the approach described in [14]. Therefore, firstly, considering that in FENNECS the discretization is performed with upright triangular prisms as finite elements, Eq. (3) and (4) must be multiplied by the test functions $\varphi^T(\vec{r}) = (\varphi_1(\vec{r}), \ \ldots, \ \varphi_6(\vec{r}))^T$. Secondly, integration over the volume Γ^e of the triangular prismatic finite element e is performed. Thirdly, the Gauss theorem is applied to transform second order to first order spatial derivatives. Then, $F_{0,g}$ and $F_{1,g}$ must be expanded in terms of the basis functions as

$$F_{k,g}(\vec{r}) = \sum_{j=1}^{6}\varphi_j(\vec{r})f^e_{k,g,j} = \begin{pmatrix}\varphi_1(\vec{r})\\ \vdots \\ \varphi_6(\vec{r})\end{pmatrix}\cdot\begin{pmatrix}f^e_{k,g,1}\\ \vdots \\ f^e_{k,g,6}\end{pmatrix} = \vec{\varphi}(\vec{r})\overrightarrow{f^e_{k,g}}, \forall\, \vec{r} \in e, k = 0,1 \tag{8}$$

Consequently, the Galerkin formulation of the SP_3 approximation takes the following form:

$$\left[D_{0,g}^{e}\mathrm{d}+\left(\Sigma_{t,g}^{e}-\Sigma_{s,0,gg}^{e}\right)c-\sum_{h=1}^{5}\left(-\frac{\beta_{0,h}^{e}}{\gamma_{h}^{e}}\right)p\right]\overrightarrow{f_{0,g}^{e}}=$$
$$c\left[\frac{\chi_{g}}{k_{eff}}\sum_{g'=1}^{G}\vartheta\Sigma_{f,g'}^{e}\left(\overrightarrow{f_{0,g'}^{e}}-2\overrightarrow{f_{1,g'}^{e}}\right)+\sum_{g'=1,g'\neq g}^{G}\Sigma_{s,0,g'g}^{e}\left(\overrightarrow{f_{0,g'}^{e}}-2\overrightarrow{f_{1,g'}^{e}}\right)\right]+ \quad (9)$$
$$\left[2\left(\Sigma_{t,g}^{e}-\Sigma_{s,0,gg}^{e}\right)c+\sum_{h=1}^{5}\left(-\frac{\alpha_{0,h}^{e}}{\gamma_{h}^{e}}\right)p\right]\overrightarrow{f_{1,g}^{e}}$$

$$\left\{D_{1,g}^{e}\mathrm{d}+\left[\frac{4}{3}\left(\Sigma_{t,g}^{e}-\Sigma_{s,0,gg}^{e}\right)+\frac{5}{3}\left(\Sigma_{t,g}^{e}-\Sigma_{s,2,gg}^{e}\right)\right]c-\sum_{h=1}^{5}\left(-\frac{\alpha_{1,h}^{e}}{\gamma_{h}^{e}}\right)p\right\}\overrightarrow{f_{1,g}^{e}}=$$
$$-\frac{2}{3}c\left[\frac{\chi_{g}}{k_{eff}}\sum_{g'=1}^{G}\vartheta\Sigma_{f,g'}^{e}\left(\overrightarrow{f_{0,g'}^{e}}-2\overrightarrow{f_{1,g'}^{e}}\right)+\sum_{g'=1,g'\neq g}^{G}\Sigma_{s,0,g'g}^{e}\left(\overrightarrow{f_{0,g'}^{e}}-2\overrightarrow{f_{1,g'}^{e}}\right)\right]+ \quad (10)$$
$$\left[\frac{2}{3}\left(\Sigma_{t,g}^{e}-\Sigma_{s,0,gg}^{e}\right)c+\sum_{h=1}^{5}\left(-\frac{\beta_{1,h}^{e}}{\gamma_{h}^{e}}\right)p\right]\overrightarrow{f_{0,g}^{e}}$$

where

$$d=\int_{\Gamma^{e}}\nabla\varphi(\vec{r})\nabla\varphi^{T}(\vec{r})\,dV,\ \forall\,\vec{r}\in e \quad (11)$$

$$c=\int_{\Gamma^{e}}\varphi_{i}(\vec{r})\varphi_{j}(\vec{r})\,dV,\ \forall\,\vec{r}\in e \quad (12)$$

$$p=\int_{\partial\Gamma^{e}}\nabla\varphi(\vec{r})\varphi^{T}(\vec{r})dA,\ \forall\,\vec{r}\in e. \quad (13)$$

The terms $\sum_{h=1}^{5}\left(-\frac{\beta_{0,h}^{e}}{\gamma_{h}^{e}}\right)$, $\sum_{h=1}^{5}\left(-\frac{\alpha_{0,h}^{e}}{\gamma_{h}^{e}}\right)$, $\sum_{h=1}^{5}\left(-\frac{\alpha_{1,h}^{e}}{\gamma_{h}^{e}}\right)$, and $\sum_{h=1}^{5}\left(-\frac{\beta_{1,h}^{e}}{\gamma_{h}^{e}}\right)$ describe the boundary condition at the five faces of the finite element and their values are listed in Table 1.

Table 1: Values for $1/\gamma_{h}^{e}$, $\beta_{0,h}^{e}$, $\beta_{1,h}^{e}$, $\alpha_{0,h}^{e}$ and $\alpha_{1,h}^{e}$ depending on the boundary condition.

	$1/\gamma_{h}^{e}$	$\beta_{0,h}^{e}$	$\beta_{1,h}^{e}$	$\alpha_{0,h}^{e}$	$\alpha_{1,h}^{e}$
Interface boundary condition: $\partial\Gamma_{h}^{e}\in\partial\Gamma^{I}$	0	0	0	0	0
Vacuum boundary condition: $\partial\Gamma_{h}^{e}\in\partial\Gamma^{V}$	1/8	4	−1	−3	7
Reflective boundary condition: $\partial\Gamma_{h}^{e}\in\partial\Gamma^{R}$	1	0	0	0	0
Zero flux boundary condition: $\partial\Gamma_{h}^{e}\in\partial\Gamma^{ZF}$	∞	4	−1	−3	7

4 VALIDATION WITH ACADEMIC EXERCISES

The first part of the solver validation process consists in testing it on simple models. For this reason, academic exercises are particularly suited. Two examples will be analysed here. The first one is constituted by quadratic fuel assemblies and the second one by hexagonal ones.

4.1 Cartesian benchmark

The geometry description and cross sections of the Cartesian benchmark are given in [15], where this is modelled with the SP_3 solver of TRIVAC, a modular neutronic code for design applications and fuel management [15,16]. This benchmark is a small two-dimensional core with vacuum boundary conditions, having assemblies with a pitch of 40 cm, made of fuel, reflector and a pure absorber that are disposed concentrically, as depicted in Figure 1. Due to its small size and the strong variation between the material properties, it is particularly suited to show the limitations of the diffusion theory and to demonstrate the performance of the SP_3.

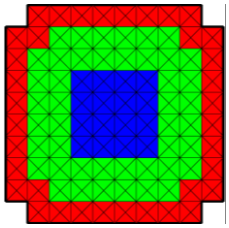

Figure 1: Mesh of the Cartesian benchmark with 4 radial elements per assembly. The blue, green, and red regions are composed by fuel, reflector, and pure absorber, respectively. The thick black lines represent the vacuum boundary condition.

The calculations were performed with the SP_3 and the diffusion solver of FENNECS with different meshes. The obtained multiplication factors are compared to the ones from the TRIVAC SP_3 solver based on the Raviart–Thomas zeroth order (RT0) solution with analytical integration (AI) and with Gauss-Legendre quadrature (GLQ). As in [15], the reference used is k_{eff} = 0.992160, which was calculated by the TRIVAC SP_5 solver based on the Raviart–Thomas second order (RT2) solution with GLQ and 16 radial elements per assembly.

As shown in Table 2, the discrepancies between the multiplication factors of TRIVAC and FENNECS and the reference value, were evaluated. In the case of the FENNECS diffusion solver, the disagreements are striking: for 4 as well as for 16 radial elements per assembly the difference is above 4300 pcm. This result clearly shows that the diffusion approximation is not well suited to model such very small cores. However, these high discrepancies should be further investigated. If the cross sections would have been generated with Serpent, and not already given, it would have been possible to apply the superhomogenization (SPH) method [17], from which an improvement of the results is expected.

Table 2: Multiplication factors for the Cartesian benchmark from FENNECS and TRIVAC with their deviations from TRIVAC SP_5 RT2 GLQ with 16 radial elements per assembly.

Program	Solver	Radial elements per assembly	k_{eff}	Difference with the reference (pcm)
FENNECS	Diffusion	4	0.94575	-4946
		16	0.95129	-4330
	SP_3	4	0.98079	-1168
		16	0.98793	-432
		36	0.98960	-261
		64	0.99024	-195
		144	0.99073	-145
		400	0.99099	-119
		2116	0.99112	-106
TRIVAC RT0 AI	SP_3	4	0.995780	366
		16	0.992535	38
		36	0.991794	-37
TRIVAC RT0 GLQ	SP_3	4	0.989783	-242
		16	0.990796	-139
		36	0.990989	-119

The results from the FENNECS SP_3 solver show smaller discrepancies and the agreement with the reference drastically increases by reducing the mesh size: with 2116 radial elements per assembly the discrepancy is only 106 pcm. At this point, mesh refinement does not affect the k_{eff}. On the contrary, increasing the number of elements from 4 to 16, leads to significant improvements: the discrepancy is halved. Regarding the better agreement of TRIVAC with the reference, this can be explained by the use of AI or GLQ, hence more accurate methods.

4.2 Hébert benchmark

The Hébert benchmark, depicted in Figure 2, is very similar to the exercise above. The main difference are the hexagonal assemblies, having a pitch of 32.9 cm. Here, the comparison is performed between results calculated by FENNECS and the ones from the SP_3 solvers of DYN3D and of TRIVAC, which were taken from [13], together with the cross sections.

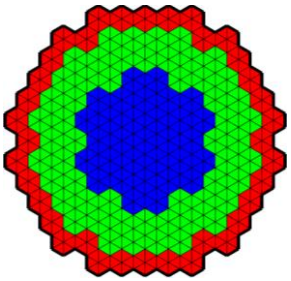

Figure 2: Mesh of the Hébert benchmark with 6 radial elements per assembly. The blue, green, and red regions are composed by fuel, reflector, and pure absorber, respectively. The thick black lines represent the vacuum boundary condition.

Table 3 shows the multiplication factors and their deviations from the reference, which is the TRIVAC SP_3 solver, where k_{eff} = 1.000332. Here, it can be observed that the discrepancies between the k_{eff} from the FENNECS diffusion solver and the reference are again above 4300 pcm. Also here, if Serpent generated cross section would have been used, the SPH method could have been applied, from which a decrease of the discrepancy is expected.

Table 3: Multiplication factors for the Hébert benchmark from FENNECS and DYN3D and their deviation from TRIVAC SP_3 reference.

Program	Solver	Radial elements per assembly	k_{eff}	Difference with the reference (pcm)
FENNECS	Diffusion	6	0.95641	4590.9
		24	0.95845	4368.3
	SP_3	6	0.99533	502.4
		24	0.99861	172.4
		96	0.99975	58.2
		384	1.00009	24.2
		1536	1.00019	14.2
		2166	1.00021	12.2
DYN3D	SP_3	6	1.001100	-76.7
		24	1.000085	24.7
		96	0.999939	39.3
		384	1.000039	29.3
		1536	1.000156	17.6
		6144	1.000238	9.4

For both SP_3 solvers, the discrepancies are drastically smaller: the difference between the reference and the k_{eff} from the FENNECS SP_3 solver with 6 radial elements per assembly is only 502.4 pcm, whereas for the SP_3 solver of DYN3D it is -76.7 pcm, hence it is lower. However, refining the mesh, the k_{eff} of FENNECS and DYN3D approach closer the reference. In particular, with the SP_3 solver of FENNECS, a larger improvement can be observed compared to DYN3D, such that starting from 384 radial elements per assembly, the k_{eff} from FENNECS SP_3 is closer to the reference, compared to DYN3D. Therefore, the methodology of FENNECS SP_3 shows a stronger dependency on the mesh, compared to the one of DYN3D.

For this benchmark, also the normalized flux distributions from the SP_3 solvers of FENNECS and DYN3D are evaluated and compared to the TRIVAC SP_3 reference. In Table 4, the root mean squared (RMS) and the maximum and minimum deviation for the distributions of the deviations from the reference of the normalized neutron flux can be found. Here, it can be observed that with a small number of radial subdivisions the normalized flux distributions from DYN3D are closer to the reference, compared to FENNECS, as seen from the RMS and the maximum deviations and as it can observed in Figure 3. For both solvers, the RMS and the maximum errors decrease with the mesh refinement. However, as it was the case for the k_{eff}, this decrease is stronger for FENNECS: starting from 96 radial elements per assembly, the SP_3 solver of FENNECS yields a normalized flux distribution closer to TRIVAC, compared to DYN3D, as stated by the RMS and the maximum deviation and as it can be seen in Figure 4.

Table 4: RMS (%), maximum and minimum deviations of the normalized neutron flux distributions, depending on mesh, with respect to the reference.

Radial elements per assembly	RMS (%)		Maximum (%)		Minimum (%)	
	FENNECS SP_3	DYN3D SP_3	FENNECS SP_3	DYN3D SP_3	FENNECS SP_3	DYN3D SP_3
6	4.1	1.7	8.3	-2.5	0.2	0.0
24	1.5	1.1	3.2	-1.9	0.0	0.0
96	0.5	0.6	1.0	-1.4	0.0	0.1
1536	0.1	0.2	-0.3	-0.5	0.0	0.0

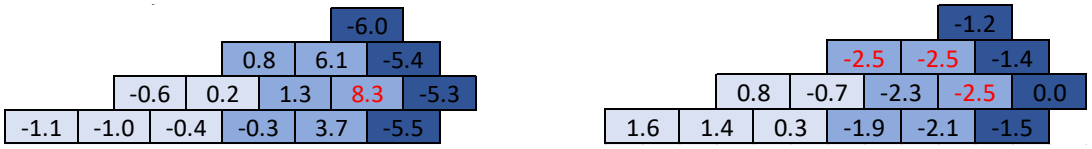

Figure 3: Deviations (%) from the reference of the normalized neutron flux distributions for the SP_3 solvers of FENNECS (left) and DYN3D (right) with 6 radial elements per assembly. The red numbers are the maximum deviations.

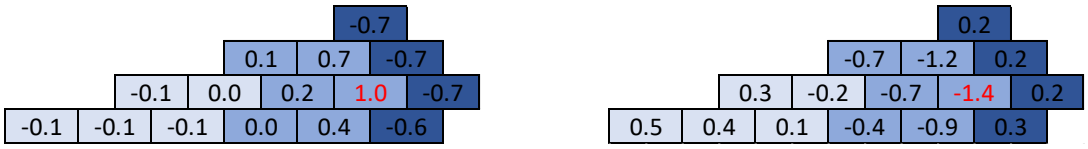

Figure 4: Deviations (%) from the reference of the normalized neutron flux distributions for the SP_3 solvers of FENNECS (left) and DYN3D (right) with 96 radial elements per assembly. The red numbers are the maximum deviations.

5 CONCLUSIONS

In this work, starting from neutron transport theory, the equations of the SP_3 approximation in the Galerkin formalism were derived. The equations obtained were used to implement an SP_3 solver in the deterministic finite element neutronic code FENNECS.

The functionality of the solver was demonstrated with the Cartesian and with the Hébert benchmarks. In the first one, the k_{eff} was used to prove the superiority of the SP_3 approximation with respect to diffusion theory for a small heterogeneous core. In the second one, the k_{eff} as well as the normalized flux distributions of FENNECS and DYN3D were compared to TRIVAC SP_3. Here, it could be observed, that the SP_3 solver of DYN3D yields better results for coarse meshes. However, a mesh refinement leads to a significant improvement of the results from the FENNECS SP_3 solver, such that for a finer meshes these are closer to the

reference compared to the ones of DYN3D. In the near future, the verification and validation work will be continued on more realistic test cases, e.g. PWR fuel assemblies and SFR cores.

ACKNOWLEDGMENTS

This work was supported by the German Federal Ministry for the Environment, Nature Conservation, Nuclear Safety and Consumer Protection.

6 REFERENCES

[1] E. Science, Deterministic Numerical Methods for Unstructured-Mesh Neutron Transport Calculation, Elsevier Science & Technology, San Diego, 2021.
[2] A.M.G. Cox, S.C. Harris, E.L. Horton, A.E. Kyprianou, Multi-species Neutron Transport Equation, Journal of Statistical Physics 176 (2019) 425–455.
[3] P.S. Brantley, E.W. Larsen, The Simplified P3 Approximation, Nuclear Science and Engineering 134 (2000) 1–21.
[4] A.V. Avvakumov, V.F. Strizhov, P.N. Vabishchevich, A.O. Vasilev, Numerical modeling of neutron transport in SP3 approximation by finite element method, http://arxiv.org/pdf/1903.11502v1.
[5] Ö. Ege, V. Öztürk, A. Bülbül, Diffusion Approximation to Neutron Transport Equation with First Kind of Chebyshev Polynomials, SDU Journal of Science 2015 (2015) 92–96.
[6] W.M. Stacey, Nuclear reactor physics, 2. ed., completely rev. and enlarged., WILEY-VCH, Weinheim, 2007.
[7] S. Marguet, The Physics of Nuclear Reactors, Springer International Publishing, 2018.
[8] Y. Wu, Neutronics of Advanced Nuclear Systems, Springer, Singapore, 2019.
[9] Q.-Q. Pan, T.-F. Zhang, X.-J. Liu, H. He, K. Wang, SP3-coupled global variance reduction method based on RMC code, NUCL SCI TECH 32 (2021).
[10] J. Bousquet, A. Seubert, R. Henry, New finite element neutron kinetics coupled code system FENNECS/ATHLET for safety assessment of (very) Small and Micro Reactors, J. Phys.: Conf. Ser. (2020).
[11] A. Seubert, J. Bousquet, R. Henry, RECENT ADVANCES OF THE FENNECS NEUTRONICS CODE FOR SAFETY ASSESSMENT OF (V)SMR, GENERATION IV AND OTHER INNOVATIVE CONCEPTS, in: The International Conference on Mathematics and Computational Methods Applied to Nuclear Science and Engineering: Proceedings, Raleigh, North Carolina, 2021.
[12] E.E. Lewis, W.F. Miller, Computational methods of neutron transport, Wiley, New York, 1984.
[13] S. Dürigen, Neutron Transport in Hexagonal Reactor Cores Modeled by Trigonal-Geometry Diffusion and Simplified P3 Nodal Methods (2013).
[14] A. Seubert, A 3-D FINITE ELEMENT FEW-GROUP DIFFUSION CODE AND ITS AP-PLICATION TO GENERATION IV REACTOR CONCEPTS, in: Proceedings of PHYSOR 2020, Cambridge, United Kingdom, 2020.
[15] A. Hébert, Mixed-dual implementations of the simplified method, Annals of Nuclear Energy 37 (2010) 498–511.
[16] A. Hebert, Trivac: A Modular Diffusion Code for Fuel Management and Design Applications, Nuclear journal of Canada (1987) 325–331.
[17] A. Hebert, A Reformulation of the Transport-Transport SPH Equivalence Technique, Proceedings 7th International Conference on Modelling and Simulation in Nuclear Science and Engineering (7ICMSNSE), Ottawa, Ontario, Canada (2015).